CrossMark

REGULAR ARTICLE

A biomechanical model for maize root lodging

Philip F. Brune (iD) · **Andy Baumgarten** · **Steve J. McKay** ·
Frank Technow · **John J. Podhiny**

Abstract

Background and aims Root lodging is a structural failure of the root-soil anchorage system in a plant that adversely affects its yield. It is a complex phenomenon that depends strongly on both crop genetics and environmental factors. An accurate biomechanical model to predict root lodging would disentangle the component factors and improve development of lodging resistant plants, thereby reducing the constraint of root lodging on crop yields.

Methods We developed a biomechanical model that employs an engineering safety factor approach to quantify root lodging resistance as the ratio of anchorage supply and wind demand. We also conducted field experiments to parametrize the model for a sensitivity analysis and validate the model for predictive accuracy.

Results The sensitivity analysis revealed primary, secondary, and tertiary factors for root lodging. The primary factors consisted of root angle, structural rooting depth, soil strength, and wind speed. The secondary factors were plant height, ear height, leaf area, stalk taper, ear mass, and leaf drag. Tertiary factors were stalk diameter and leaf number. The validation analysis found the model predictions compared well with data collected from three natural lodging events, with a goodness-of-fit of 0.58.

Conclusions The model effectively described a collection of natural lodging events, giving confidence in its predictive accuracy as well as the relative phenotypic and envirotypic influence factors determined in the sensitivity analysis. There are significant opportunities for model improvement, perhaps most significantly in the phenomenological understanding of the physical process.

Keywords Maize · lodging · anchorage · aerodynamics · soil strength

P. F. Brune (✉) · A. Baumgarten · S. J. McKay ·
F. Technow
DuPont Pioneer, Johnston, IA, USA
e-mail: PBrune@gmail.com

J. J. Podhiny
Materials Research & Design, Wayne, PA, USA

Introduction

Root lodging is defined as the irreversible mechanical deformation of a plant's subterranean support structure.[1] It is a physical process by which wind action on a plant's above-ground structure generates an aerodynamic load whose resultant bending moment surpasses the root-soil anchorage capacity, causing a rotation of the below-ground support base and angling the plant from vertical (Niklas 1992). Yield losses are inevitable, in terms of reduced crop harvestability and/or diminished grain size, number, and quality. Root lodging afflicts a variety of cereal crops. Broader scientific efforts have focused on wheat (*Triticum aestivum L.*), barley (*Hordeum*

---

[1] Not to be confused with goose-necking, a biological process through which above-ground plant organs recover their verticality following a root lodging event through phototrophic growth.

Springer

vulgare L.), sunflower (*Helianthus annuus L.*), and oats (*Avena sativa L.*) (Pinthus 1973; Berry et al. 2004). The present work focuses on maize (*Zea mays L.*), for which there is less preceding scholarship on root lodging of fully intact plants.[2] With some exceptions (Carter and Hudelson 1988; Stamp and Kiel 1992), much of the work involves roots that have been variously compromised by corn root worm (*e.g.* Spike and Tollefson 1991).

Accurate modeling of the root lodging event requires careful representation of the relevant physical phenomenology. Dynamic amplification is an essential component in the mechanical excitation of (plant) structures by wind. A steady wind at constant velocity blowing on a stably supported object applies a 'static' aerodynamic force through drag. If occasional gusts are superimposed atop the steady wind, then additional dynamic forces can significantly increase the load on the structure if the interval of the gusts excites a resonant frequency of the structure. In this case, the periodic dynamic loads cause large oscillatory displacements of the structure that significantly amplify the mechanical load on the structure and its supports. Oliver and Mayhead (1974) in their work on Scots pine (*Pinus sylvestris L.*) identified dynamic amplification as explaining the discrepancy between measured wind speeds during a destructive storm and the failure wind speeds calculated from an aerostatic interpretation of forces necessary to mechanically overturn trees in the same forest. Blackburn and Petty (1988) extended the methodology in their study of Sitka spruces (*Picea sitchensis (Bong.) Carr.*) by instrumenting trees with accelerometers to quantify tree deflection during a storm, and found that periodic gusts dynamically amplified wind loads on the tree. Supplementing the calculated aerostatic loads with the measured dynamic load factors provided a realistic description of the failure event.

For row crops, Flesch and Grant (1991) made similar in-canopy measurements of wind speed and structural oscillation of maize plants, with computed transfer functions showing a clear increase of the wind-induced flexure by excitation frequencies close to the resonant frequency of the individual plants (~1 Hz). Sterling et al. (2003) employed a portable wind tunnel with fans controlled to approximately reproduce velocity spectra and quadrant hole analysis of Reynolds stress obtained from

three-dimensional anemometer measurements during a lodging event (Lu and Willmarth 1974). Application of the airflow patterns to wheat plants instrumented with strain gauges verified the structural response of the plants to be that of a damped harmonic oscillator, with behavior characterized by dynamic vibration properties. These investigations focused on the dynamic character of the plant structural response to in-canopy turbulent airflow; investigations that analytically described the interaction between plant canopy and turbulent airflow are acknowledged as providing essential foundations to understanding how to represent the mechanical stimulus that induces failure (*e.g.* Raupach and Thom 1981, Raupach et al. 1996, Finnigan 2000).

The interaction of roots and soil to provide mechanical anchorage is the other key physical component needed to accurately model root lodging. Coutts (1983) applied an engineering approach to extend the work of Waldron (1977) and quantify the anchorage of Sitka spruces in terms of the constituent root and soil mechanical strength properties. A sequential failure process was identified, with the mechanisms of leeward plastic hinge formation, soil shear failure, and windward root pull-out and fracture variously superposed during the overturning process to account for the total measured bending resistance. Ennos et al. (1993) extended the approach to maize, supplementing a mechanistic description of the root lodging process with biomechanical measurements of the stiffness and strength of subterranean crown roots. The primary anchorage failure mode was identified as a buckling of leeward roots, while mechanical testing of roots revealed a strong tapering effect resulting in significant decreases in flexural properties with distance from the base of the root. A subsequent investigation by Goodman and Ennos (1999) confirmed the importance of soil strength to plant anchorage by measuring a greater resistance to mechanically induced lodging by plants in soil that had larger shear strength via increased bulk density.[3]

This collection of physical phenomenology provides a basis for the biomechanical model. Its development follows that of several preceding efforts, most notably the work in Baker (1995) and Baker et al. (1998). These contributions are individually cited with the components

---

[2] 'Fully intact' refers to plants whose roots systems have not been reduced by root worm feeding.

[3] Note: results were obtained for a single growth medium, a reconstituted mixture of sandy loam top soil, peat, and sand in 7:3:2 volumetric proportion (Goodman and Ennos 1999).

of the model they pertain to in the following section, which details the model development process. A description of the validation field experiments is then followed by results and discussion, and lastly conclusions.

Model development (materials & methods)

The biomechanical model applied an engineering safety factor approach to quantifying the proximity of a single maize plant to root lodging failure. The model computed the anchorage supply provided by the interaction between roots and soil, and the wind demand originating from the interaction of the wind and above-ground plant structure. The plant's non-dimensional root lodging resistance (RLR) was defined as the ratio of the computed anchorage supply (AS) and wind demand (WD):

$$RLR \equiv AS/WD \tag{1}$$

Both AS and WD were directly computed by sub-models as equivalent bending moments [N*mm]. Salient details of each sub-model appear in the following sub-sections.

Wind demand sub-model

The WD sub-model followed one of the approaches introduced in Baker (1995) and expanded in Baker et al. (2014) of adopting a spectral representation of the airflow and its resulting aerodynamic loads. Instead of a closed-form analytical approach, however, the model was implemented in a commercial Finite Element Analysis platform (Abaqus v6.14; Dassault Systèmes 2014). Utilizing Abaqus facilitated more sophisticated treatments of the additional complexity presented by the maize plant structure and material, specifically taper in the elliptical stalk cross-section, variously located and sized leaves, and the difference in mechanical response of internode versus node stalk tissue.[4]

Model creation started with generating the structural geometry. The stalk was the primary structure of interest, and was represented directly in the model. Key input parameters were total plant height [cm] and the locations of nodes along the stalk [% of height], defining the structural geometry of the stalk in terms of internode

lengths and node positions.[5] The stalk was discretized using structural beam elements with shear flexibility to represent the low aspect ratio (length / diameter) of stalk node (as opposed to internode) regions. The elliptical stalk cross-section and its taper with height were implemented via general beam sections. Both the node and internode material responses were defined as linear elastic. The simple material model was considered sufficient to represent the difference in node and internode material stiffness, accounted for in the model by a 3× increase to the elastic modulus [GPa] in the node sections following the measurements of stalk structural stiffness [N/m] in Robertson et al. (2014). At present, there is insufficient experimental data to support more elaborate material responses, such as those in Miller (2005) and Von Forell et al. (2015). A uniform mass density [gm/cm^3] was used for the entire stalk, as localized increases in the node sections were analytically determined not to significantly alter the responses of interest.

Other mechanically consequential features of the maize plant were represented indirectly as engineering features. Leaves were modeled by aerodynamic forces applied to the stalk nodes, with magnitudes scaled by a triangular approximation of their area [cm^2]; more detail appears subsequently in the description of the model aerodynamics. Finite root-soil stiffness was represented by a torsional spring [N*mm/rad] connected to a fixed boundary. As noted in Baker (1995), including the compliance of the roots and soil was important for accurately predicting the natural frequency [Hz] of the plant; assuming a fixed boundary condition (infinite root soil stiffness) increased the computed natural frequency by ~3×. For modeling of root lodging of mature plants, an ear was implemented as a lumped mass [gm] located at an input ear height [cm].

The aerodynamics representation approximated the transformation of turbulent wind energy into mechanical loads on the plant structure. The approach followed that of Baker (1995), combining several components to produce a spectral representation of the aerodynamic force applied by the wind to the plant. The first component was the aerostatic force F_{AS} [N], computed as:

$$F_{AS}(z) = \frac{1}{2}\rho \cdot A_A(z) \cdot Cd \cdot V_{avg}(z)^2 \tag{2}$$

with z [cm] the vertical coordinate along the stalk, ρ the mass density of air [gm/cm^3], A_A the aerodynamic area

---

[4] The difference in material response is of more consequence for stalk material failure, provisioned for a future version of the model.

[5] Each node was assigned a thickness value of 6.4 mm.

[cm^2], C_d the effective drag coefficient, and V_{avg} the average wind speed [m/s]. The aerostatic force was computed for each Finite Element Node (FEN, see Bathe 2014 for background on the Finite Element method) based on the lengths and diameters of the elements connected to it.[6] If the FEN was associated with a region in the *internode* of the stalk, the aerodynamic area was that of the associated stalk volume and the effective drag coefficient was set to the value for the stalk (C_{d_s} = 1.0), taking the value for right circular cylinders in cross-flow with a Reynolds number below 5×10^5 (Tritton 1988). If the FEN was associated with a region in the *node* of the stalk, an additional drag force associated with the leaf was superposed atop the stalk drag force. The effective drag coefficient for the leaf C_{d_l} was input using data from Wilson and Shaw (1977) and Flesch and Grant (1991). The leaf aerodynamic area was determined as a function of the height of the leaf (*i.e.* the height of the stalk node to which it was attached) using the plant area density reported by Shaw et al. (1974) scaled to the height of the plant being considered (Fig. 1a). Additionally, a drag reduction factor of 0.5 was applied to reduce the leaf forces from skin drag, reflecting measurements that streamlined bodies experience reduced drag at higher Reynolds number flows (Tritton 1988). Finally, the distribution of average wind speed was determined as a function of the height of the stalk (z) via the normalized velocity profile reported in Shaw et al. (1974). The input average wind speed from a weather station V_{avg_WS} was used to quantify the actual (as opposed to normalized) vertical distribution of average wind speed (Fig. 1b) via:

$$V_{avg}(z) = V_{avg_{WS}} \cdot exp\left(\alpha \cdot \left(\frac{z}{h_{WS}} - 1 \right) \right) \quad (3)$$

with α the exponential coefficient for a mature maize canopy (Shaw et al. 1974) and h_{WS} the height [m] of the weather station at which V_{avg_WS} was measured.

The second component used to obtain a spectral representation of the aerodynamic force was the aerodynamic admittance function Γ:

$$\Gamma(f, z)^2 = \frac{1}{1 + 2.5 \cdot \left(\frac{f \cdot D_c}{V_{avg}(z)} \right)^2} \quad (4)$$

---

[6] Briefly: in considering boundary value problems, the Finite Element method discretizes the domain into a mesh of interconnected finite elements. The vertices that define the coordinates of the elements are called nodes. They should not be confused with stalk nodes.

with f the frequency [Hz] being analyzed, V_{avg} the average wind speed, and D_c [m] the canopy diameter, which is the periodic plan view area encompassed by the plant, and is estimated from the planting density PD [plants/acre]:

$$D_c = 2\sqrt{1/PD} \quad (5)$$

The aerodynamic admittance truncated the frequency spectrum of the in-canopy turbulent airflow by removing the higher frequencies whose action does not excite the vibrational modes of the plant that determine its structural response to wind gusts (Baker 1995).

The final component used to define the force spectrum was the velocity spectrum of the wind. The Von Karman form was adopted following Baker (1995). The suitability of this choice was evaluated by Martinez-Vazquez (Martinez-Vazquez 2016, Fig. 5), which calculated good agreement with the in-canopy velocity spectrum reported in Finnigan (2000), especially over the frequency domain from 0.1-100 Hz, the area of greatest consequence for lodging inducement. The velocity power spectrum density (PSD) S_v [(m/s)^2/Hz] was expressed as:

$$S_v(f, z) = \frac{4\sigma_v^2 \cdot \left(\frac{f \cdot L_{tb}}{V_{avg}} \right)}{f \cdot \left(1 + 70.8 \cdot \left(\frac{f \cdot L_{tb}}{V_{avg}(z)} \right)^2 \right)^{5/6}} \quad (6)$$

with L_{tb} [m] the turbulence length scale and σ_v [m/s] the standard deviation of the wind speed. The velocity PSD, aerodynamic admittance, and aerostatic force were combined to calculate the aerodynamic force PSD for each FEN as S_p [N^2/Hz]:

$$S_p(f, z) = 4S_v(f) \cdot \left(\frac{F_{as}(z) \cdot \Gamma(f)}{V_{avg}(z)} \right) \quad (7)$$

The WD sub-model was run in two steps. The first step calculated the modal response of the plant. While only the lowest two vibration modes participated significantly in the dynamic response, the frequencies associated with the first four modes were calculated to be conservative. The second step applied a random response analysis that utilized the previously calculated modal response and the aerodynamic force PSD to determine the PSD of the resultant bending moment at the base of the plant B_{PSD} [(N*mm)^2/Hz]. The total effective bending moment B_{max} [N*mm] at the plant
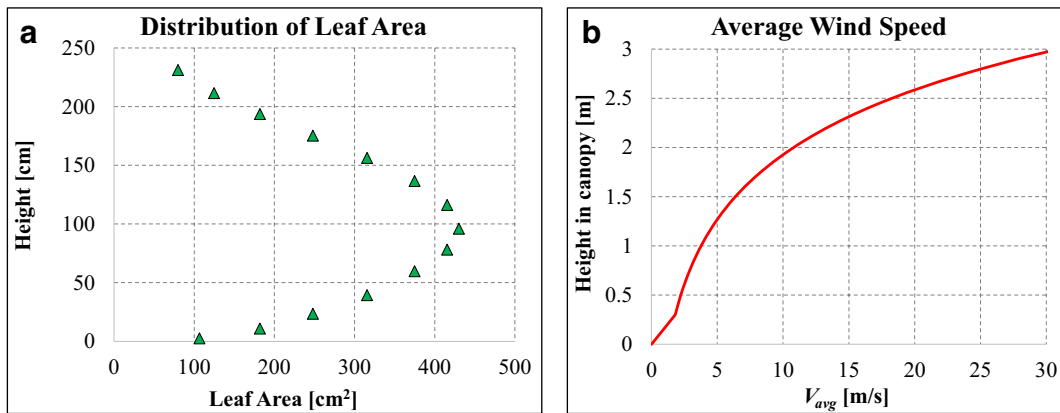
Fig. 1 a Distribution of leaf area over the height of a plant with 14 total above-ground stalk nodes, based on the distribution from Shaw et al. (1974). **b** Logarithmic distribution of the average wind-speed in a mature corn canopy, following data from Shaw et al. (1974). A linear extrapolation was used to force the wind speed to zero at ground level

base was then calculated by summing the dynamic and static contributions:

$$B_{max} = \sum_i F_{AS}(z_i)_i \cdot z_i + GF \cdot \sqrt{\int B_{PSD} df} \qquad (8)$$

The first term was the static component, obtained by summing the bending moments generated by the aero-static force applied at each FEN. The second term was the dynamic component, calculated as the root mean square of the bending moment PSD scaled by a gust factor; the gust factor was defined as a constant value of 4, following Baker (1995). The maximum bending moment is the output of the WD sub-model. Figure 2a shows a comparison between B_{PSD} calculated via the WD sub-model in Abaqus and the analytical closed-form example for wheat in Baker (1995), which was used as a validation case to ensure accurate implementation within the Finite Element analysis platform. Figure 2b shows a comparison of B_{PSD} for the wheat validation case with one calculated for a typical maize plant to emphasize the differences between the two crop architectures.

Anchorage supply sub-model

The AS sub-model followed a more straightforward mechanistic approach. It was developed from a closed-form analytical representation of the anchorage zone. The anchorage zone was modeled as a region of 'bulk' soil surrounding a hemi-spheroid of root-reinforced (RR) soil that approximated the maize root ball and was subjected to an applied bending moment (Fig. 3).

Anchorage failure was described as a rotation of the RR soil volume along the interfacial surface between bulk and RR soil. This rotation was resisted by the shear strength of the interface, assumed to be the total shear strength of the bulk soil, τ [kPa], expressed in Mohr-Coulomb form as[7]:

$$\tau = c + \sigma \cdot \tan\phi \qquad (9)$$

with c [kPa] the total cohesion, σ [kPa] the total normal stress, and φ the total internal friction angle [deg].

The proximity of the anchorage zone to the top soil surface means there is not much normal stress from overburden. Also, a lot of agricultural soils have large silt- and clay-sized fractions, making their behavior, especially at higher degrees of saturation, more cohesive. Therefore, as a first approximation, the frictional component of the shear strength was assumed to be zero, which reduced the material response of the system to a single parameter, the total cohesion of the bulk soil. Finally, a complete mobilization of a uniform shear stress was assumed at all points of the interface, and the anchorage supply was described by this shear stress assuming the value of the total shear strength, *i.e.* the cohesion of the bulk soil. A balance of moments then expressed the anchorage strength [N*mm] in closed form as:

$$AS = \frac{\pi}{4} \cdot c \cdot D_{RB}{}^3 \qquad (10)$$

---

[7] See Horn and Lebert (1994) and Wulfsohn et al. (1998) for discussion of total versus effective stress measures as pertains to agricultural soils.
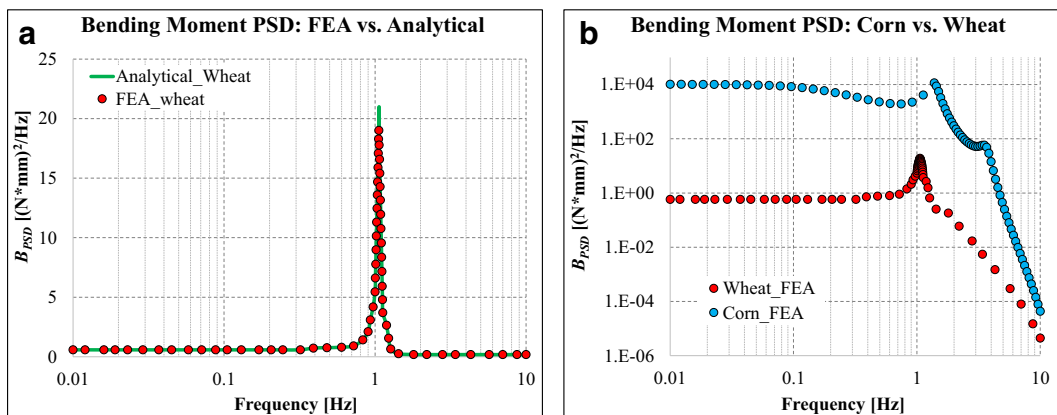
Fig. 2 **a** Plot showing agreement between analytical solution (Baker 95) and FEA solution for a single wheat shoot. **b** Plot showing difference between single wheat shoot and single corn plant

with the root ball diameter D_{RB} [mm] used to quantify the extent of the RR soil zone. Given the emphasis of the model on describing so called 'early' root lodging of maize, which occurs before flowering and development of brace roots, an equivalent sphere is an appropriate approximation for the structural morphology of the root system.

While this description of anchorage almost certainly oversimplified the problem, its form followed previous results. It agreed dimensionally with the analysis of Crook and Ennos (1993) on wheat, and was quantitatively close to the model of Baker et al. (1998) for wheat, which applied a scale factor of 0.43 to the product of the root ball diameter cubed and soil shear strength, compared with the factor of π/4 obtained here.
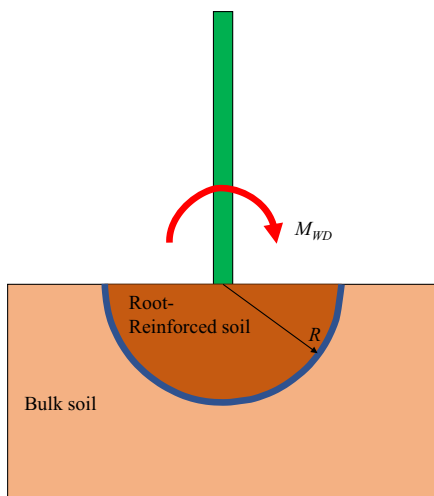

Fig. 3 Schematic showing quantities used in derivation of anchorage sub-model. The assumed failure interface is highlighted in blue as the outer extent of the root-reinforced soil region

Finally, use of this framework allowed the soil strength for most soils prone to root lodging to be reasonably estimated via *in situ* measurement with an appropriately sized shear vane.

The AS sub-model was evaluated in closed form from the input parameters, namely the proximally measured bulk soil shear strength under appropriate moisture conditions, and the excavated root ball diameter, either measured directly or calculated from measurements of the root angle RA [deg] and structural rooting depth d_{SR} [cm] via:

$$D_{RB} = 2 \cdot d_{sr} \cdot \sin\left(\frac{RA}{2}\right) \qquad (11)$$

Once calculated, the ratio of the outputs of the AS and WD sub-models, respectively, quantified the model-predicted root lodging resistance per Eq. (1).

Field validation experiments (materials & methods)

The accuracy of the root lodging model was assessed through field tests. Thirty mid-maturity maize hybrids with various phenotypic attributes and susceptibilities to root lodging were planted in randomized experimental blocks of 76.2 cm (30 in.) rows at a population density of 14,569 plants/ha (36,000 plants/acre) at three research locations (Princeton IL, Miami MO, and Dallas Center IA). Plants were managed following standard practices. All locations experienced natural root lodging events at various times before flowering, while the plants were in the vegetative growth stage of development, generally between V7-V10, i.e. with 7–10 fully developed leaves.

Plant phenotypes and location envirotypes were collected at each location following the lodging events. The severity of root lodging was measured by the field stalk angle [deg], defined as the angle from vertical of the base of the stalk (Fig. 4a) within the plane of maximum lodging. This captured the amount of rotation by the root-soil support structure, quantifying the extent of anchorage failure. Plants were scored via a two-step process. First the entire row was quickly observed to coarsely quantify the total extent of lodging on a scale of 1–4; a score of 1 was assigned when most plants were completely vertical, and a score of 4 was assigned when most plants were significantly (>30 deg) lodged. Second, three plants were identified that were representative of the coarse row-level score. The field stalk angle was measured for these individuals with a digital angle-finder or inclinometer, and the plants were flagged for subsequent root excavation.

Soil envirotypes were measured at the same time as plant phenotypes, usually around a week after the lodging event due to delays imposed by travel. Consequently, the soil data described a different moisture state than when the lodging event occurred, and relative differences between plots under similar moisture conditions were emphasized. Soil measurements were made after the field stalk angles were measured and before root excavation, in the plane of lodging, 15 cm from the stalk base of flagged plants. The distance from the plants ensured that measurements characterized bulk (rather than root-reinforced) soil properties. Two measures of *in situ* soil strength were collected. First, the soil shear strength [kPa] was estimated using a Geovane shear vane with vane dimensions of 19 mm × 38 mm, loaded at a rate of 0.8 (or, $\pi/4$) radians per second, after recommendations in ASTM D2573 (2015). The vane was inserted to a depth of 7 cm, to approximately coincide with the depth of the anchorage zone centroid. Second, the soil penetration resistance [MPa] was measured as a function of depth using an Eijkelkmap Penetrologger with a cone of 1 cm^2 base area and 60-degree angle inserted at a rate of 2 cm/s, following considerations in ASTM D3441 (2016) and D5778 (2012). Also, volumetric water content [%] of the top 6 cm was estimated via electrical permittivity measured with an ML3 Thetaprobe (Delta-T devices) connected to the penetrometer system.

Root phenotypes were measured from excavated plants. First, the top portion of each stalk was cut off just above the soil line to remove the visual indication of lodging severity, allowing subsequent root phenotypes

to be taken under "blind" experimental conditions. Next, the root ball was excavated with a digging ("potato") fork, inserted to fully cover the tines. This depth was sufficient to extract the full extent of root balls for all plants. The excavated root balls were soaked in a bucket of water for around 30 min, agitated to remove additional soil, and then characterized. Two root phenotypes were selected to describe the morphology of the root system, rather than individual roots. First, the root angle [deg] was estimated using a digital angle-finder. The timing of the lodging events meant that all excavated root systems were comprised of subterranean crown roots only; no above-ground brace (or, "prop") roots had developed. This led to subjectivity in the angle measurements, as the generally ellipsoidal shape of the excavated root systems did not readily accommodate description by Euclidean geometry. The second root phenotype, the root ball diameter, was more appropriate for these morphologies. It was measured as the horizontally oriented diameter in the plane of lodging of the quasi-ellipsoidal root zone using a ruler (Fig. 4b). Initially, two orthogonally oriented measures of diameter were made, but this practice was abandoned when it was found that the additional data generally resided within measurement error.

Several above-ground phenotypes were measured. Plant height [cm] was measured as the base of the top ("flag") leaf, using a ruler-stand.[8] The stalk diameter [mm] at the base was measured using digital calipers as the average between the major and minor axes of the elliptical cross-section. Additional diameter measures were obtained just above and just below the ear, to define the stalk taper. Leaf area [cm^2] was approximated as the area of the isosceles triangle formed by the leaf width and leaf length. Sampled leaves were selected at heights nearby where the ear height had been measured in previous seasons, to provide a data point close to the maximum area denoted in the distribution of Fig. 1a. Finally, several meteorological envirotypes were collected in the form of hourly measurements of precipitation [cm], average wind speed [m/s], and air temperature [°C] made by a standard Davis Vantage Pro weather station with tipping bucket rain gauge, cup and ball anemometer, and thermocouple, respectively.

---

[8] Ear height was not measured, as the plants had lodged before development of any significant ear.

Fig. 4 **a** Schematic illustrating the field stalk angle (θ), measured at the base of the plant and used to quantify the severity of lodging. **b** Photograph showing excavated root ball (shaded red) and estimated root ball diameter
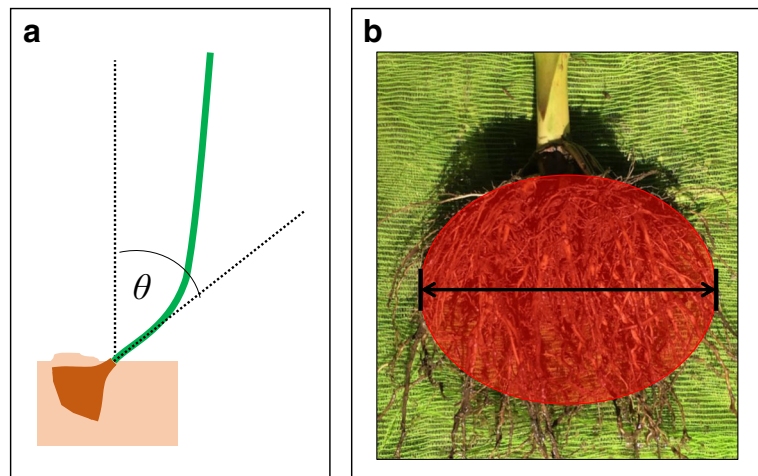
Results

Results focused on the sensitivity and validation analyses. For both analyses, select phenotypes and envirotypes gathered from the field were assembled as inputs, while other input parameters were held constant at an assumed value due to lack of available data. Table 1 presents an exhaustive list of all input parameters, and categorizes them as either varying or fixed. Input parameters were obtained by the authors per the methods and materials section, with the following exceptions taken from published values: leaf drag (Flesch and Grant 1991), stalk drag (Tritton 1988), turbulence length scale (Baker 1995), and the flexural moduli (Goodman and Ennos 1996). Changes to the varying input parameters depended on whether the analysis was intended to determine phenotypic influence on lodging resistance ('sensitivity') or evaluate model functionality in predicting field lodging events ('validation'), as further described in the following.

In the sensitivity analysis, all but one of the varying input parameters were held constant at their mean values while parameter of interest sequentially traversed the full range of its measured values. This allowed the model-predicted root lodging resistance to be calculated as a function of only the single varying input parameter. This was done for all varying input parameters, quantifying the sensitivity of the model to each one. Sensitivity analysis results appear in Fig. 5, which plots model-predicted root lodging resistance versus the normalized range of

the phenotypes and envirotypes. Values in the normalized intervals $x^{(n)}_i$ were calculated as:

$$x^{(n)}_i = \frac{x_i - min(x)}{max(x) - min(x)} \qquad (12)$$

with x_i the value of the phenotype or envirotype being normalized.

In the validation analysis, the varying input parameters took on the field-measured values for the hybrid being evaluated. All phenotypes and envirotypes were calculated as unweighted arithmetic means across the locations where they were collected. It is noted that results for some phenotypes and envirotypes at some locations were excluded from model validation due to data quality issues. Others that were difficult to measure and found not to be influential from the sensitivity study were kept constant at their average values from the sensitivity analysis, so as not to influence the ability of the model to describe the variability in root lodging response; treatment of input parameters is detailed in Table 1. Validation analysis results appear in Fig. 6, which plots the average field stalk angle measured for each hybrid across the three locations versus the root lodging resistance for that hybrid computed by the biomechanical model.

Discussion

The sensitivity analysis suggests that root lodging resistance is dominated by the anchorage components. This

Table 1 Complete list of model input parameters, typical values, physical units, and category as varying or fixed

Property	Typical Value	Unit	Category	Property	Typical Value	Unit	Category
Plant Height	275	cm	Varying	Avg wind speed	15	m/s	Varying
Ear Height	105	cm	Varying	Wind speed stdev	1.5	m/s	Fixed
Leaf Area	430	cm2	Varying	Turbulence length scale	1.5	m/s	Fixed
Leaf Drag	0.15	1	Varying	Soil strength	20	kPa	Varying
Total Leaf Number	13	1	Varying	Canopy diameter	30	cm	Fixed
Stalk Drag	1	1	Fixed	Root angle	75	deg	Varying
Ear Mass	175	gm	Varying	Root depth	8	cm	Varying
Stalk Diameter	22	mm	Varying	Air mass density	1.25E-03	gm/cm^3	Fixed
Daily rainfall	4	cm	Varying	Internode flexural modulus	1800	MPa	Fixed
Damping ratio	0.1	1	Fixed	Node flexural modulus	4500	MPa	Fixed

is seen from Table 2, which quantifies the influence of the phenotypes and envirotypes on root lodging resistance via the best fit linear slope of each curve in Fig. 5. The three anchorage components of root angle (99), root depth (94), and soil strength (80) were more influential than the primary wind demand component of wind speed (−73), while the most influential above-ground phenotypes of plant height (−23), leaf drag coefficient (−21), and ear height (−18) were clustered together as secondary effects.[9] This appears reasonable; the structural response of long, thin structures is often dominated by changes in boundary conditions. However, the relatively low values for leaf area (−8) and total leaf number (−1) suggest that the aerodynamic contributions of the leaves may have been suppressed by the drag reduction factor or insufficiently large values of the leaf drag coefficient, which was found to have more influence. Indeed, both Sposaro et al. (2010, Fig. 6a) and Berry et al. (Berry et al. 2003, Fig. 5b) showed a more pronounced effect of roughly equivalent phenotypes (gust-loaded area and shoot number, respectively) on root lodging resistance. It is possible that a plant-scale drag coefficient to represent an entire plant may be more appropriate, although the organ-scale description of drag has the benefit of incorporating phenotypic attributes that relate to other functions of the plant, such as leaf area and photosynthesis. In either approach, accurate experimental data is necessary to improve selection of drag coefficient values. Those adopted from Wilson and Shaw (1977)

were calculated as part of an investigation that targeted canopy roughness and airflow patterns; dedicated measurements of drag coefficients in airflow with Reynolds numbers around those expected for lodging inducement would improve the situation.

The validation analysis indicated that the biomechanical model described well the variation of natural root lodging measured in the field experiments. A negative linear relationship between the severity of lodging as quantified by the measured field stalk angle and model-computed lodging resistance was expected, and found to describe the data effectively. The residual of the linear trendline was evenly distributed over the range of comparison, showing little bias toward either highly resistant or susceptible genetics. This contrasted with the
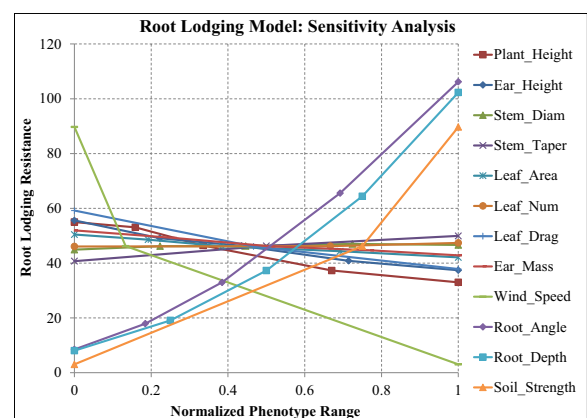

Fig. 5 Results of sensitivity analysis showing the phenotypic and envirotypic influence on root lodging resistance as predicted by the biomechanical model using input parameters with ranges shown in Table 1. Above-ground parameters are clustered together, see Table 2 for linear slope values

---

[9] Ear height was included in the sensitivity analysis to gauge its effect, as well as that of ear mass. It was not included in the validation analysis because the plants were still in vegetative states when lodging occurred.
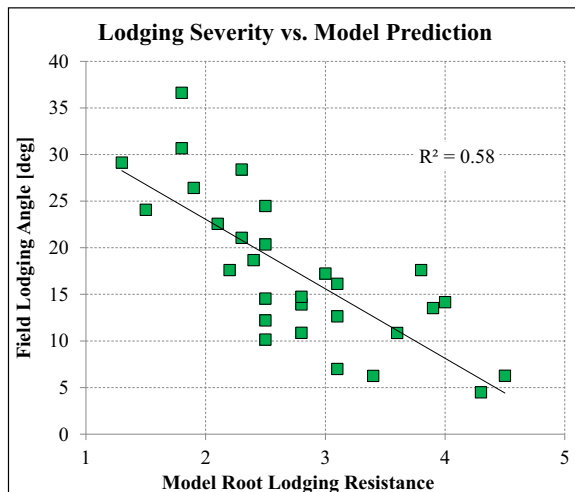
Fig. 6 Results of validation analysis showing field-measured lodging severity for each hybrid plotted versus the biomechanical model-predicted root lodging resistance. Data for the lodging severity and phenotypic inputs are averaged over the three locations

Table 2 Best fit linear slopes of the curves from Fig. 5

Model Parameter	Influence
Root Angle	99
Root Depth	94
Soil Strength	80
Average Wind Speed	−73
Plant Height	−23
Leaf Drag Coefficient	−21
Ear Height	−18
Ear Mass	−9
Stalk taper	9
Scaled Leaf Area	−8
Stalk Base Diameter	2
Total Leaf Number	1

validation results for a wheat lodging model from Berry et al. (2003, Fig. 6), which showed a notable difference in predictive accuracy between lodging resistant (poor accuracy) and susceptible (very good accuracy) varieties.[10] It is difficult to compare the model performance with that of lodging models for sunflower (Sposaro et al. 2010, Fig. 5) and barley (Berry et al. 2006, Table 3), as both reported model predictions in terms of failure wind speeds rather than actual lodging severity.

In general, these and other crop lodging models that produce failure wind speeds are difficult to validate. Measurements of wind speed depend strongly on sample rate and digital signal processing approaches to reduce measured data into descriptive parameters. Berry et al. (2000) first adopted the failure wind speed approach, quantifying wind speed as the speed of a gust with duration of at least 0.25 s, based on the assumption that for failure to occur, the plant would need to achieve maximum deflection, equivalent to one quarter of a complete period of oscillation at its first fundamental frequency of ~1 Hz This formulation requires measurement of wind speeds at much high frequencies than typically collected, complicating the validation process.

Validation of the present model suggests that the form of the anchorage sub-model (Eq. 10) is appropriate as an initial approximation. The product of a measure of soil strength and an estimate of the size of the root volume has been experimentally justified for barley (Berry et al. 2006), sunflower (Sposaro et al. 2010), and wheat (Griffin 1998). The importance of root architectural parameters in contributing anchorage resistance in maize was presented in Liu et al. 2012. Also, there is compatibility between the soil-driven failure description of the anchorage sub-model and the field stalk angle description of lodging severity, which in effect quantifies the extent of plastic deformation along the interface between root-reinforced and bulk soil (Fig. 3). Given its importance to anchorage, the description of soil strength and its reinforcement by roots could be improved, with applications of slope stability analysis to vegetated hillsides offering potential developmental avenues (*e.g.* Stokes et al. 2009). In considering a more refined representation of the root system structural morphology, recent developments in Baker et al. (2014) to describe the anchorage of tap root systems are also worthy of consideration. Additionally, the work in Manzur et al. (2014) identifies the possible utility of extending the computation of anchorage beyond coarse descriptions of total root system morphology to incorporate mechanical properties of individual roots.

The final point of discussion concerns the objective accuracy of the model. The validation analysis (Fig. 6) computed root lodging resistance values between 1.3 and 4.5. Given the definition of root lodging resistance as a safety factor (Eq. 1), this

---

[10] It is noted that these results incorporated *both* root and stem lodging of wheat plants.

range of computed values would be associated with plants that did not experience lodging failure (but perhaps came close on the low end). This was not the case, as the field lodging angles were between 5 and 36 degrees, indicative of little to substantial levels of root lodging. Two likely factors are suggested as causing this discrepancy. First, the soil strength values (Table 1) were likely conservative, as the measurements they were based on occurred well after the soil had drained and recovered some of its shear strength. Given the direct relation between anchorage strength and soil shear strength in Eq. 10, any decrease in soil strength would significantly impact computed lodging resistance. Second, the aforementioned under-representation of leaf area likely underpredicted the wind-demand, which would decrease the computed lodging resistance for a given anchorage strength.

Conclusions

This work presented the development and validation of a biomechanical root lodging model for maize. The model was relatively accurate in describing natural root lodging events, although its objective offset from field results suggests areas for improvement in treatments of soil strength and leaf aerodynamics. Significant contributions were made in implementing the spectral approach to turbulent wind flow on plants in a Finite Element analysis, quantifying the relative phenotypic importance to root lodging in maize, and defining a more appropriate approach to validating the model output that focuses on measuring plant-based lodging outcomes rather than wind velocity. There is much additional work to be done in understanding the root lodging phenomena, especially the time scale(s) on which it occurs. The resulting mechanical loading rate(s) influence both the turbulent aerodynamics and the soil strength. Finally, further validation of the model is warranted, as root lodging is a notoriously year-dependent phenomenon. The maize root lodging model offers a sturdy platform on which to explore these and other aspects of root lodging, with the objective of reducing its occurrence to better optimize the tradeoff with yield.

References

ASTM D2573 (2015) Standard Test Method for Field Vane Shear Test in Saturated Fine-Grained Soils. ASTM International, West Conshohocken

ASTM D3441 (2016) Standard Test Method for Mechanical Cone Penetration Testing of Soils. ASTM International, West Conshohocken

ASTM D5778 (2012) Standard Test Method for Electronic Friction Cone and Piezocone Penetration Testing of Soil. ASTM International, West Conshohocken

Baker CJ (1995) The development of a theoretical model for the windthrow of plants. J Theor Biol 175:355–372

Baker CJ, Berry PM, Spink JH, Sylvester-Bradley R, Griffin JM, Scott RK, Clare RW (1998) A method for the assessment of the risk of wheat lodging. J Theor Biol 194:587–603

Baker CJ, Sterling M, Berry P (2014) A generalised model of crop lodging. J Theor Biol 363:1–12

Bathe KJ (2014) Finite element procedures. KJ Bathe, Watertown

Berry PM, Griffin JM, Sylvester-Bradley R, Scott RK, Spink JH, Baker CJ, Clare RW (2000) Controlling plant form through husbandry to minimize lodging in wheat. Field Crop Res 67: 59–81

Berry PM, Sterling M, Baker CJ, Spink J, Sparkes DL (2003) A calibrated model of wheat lodging compared with field measurements. Agric For Meteorol 119:167–180

Berry PM, Sterling M, Spink JH, Baker CJ, Sylvester-Bradley R, Mooney SJ, Tams AR, Ennos AR (2004) Understanding and Reducing Lodging in Cereals. Adv Agron 84:217–271

Berry PM, Sterling M, Mooney SJ (2006) Development of a model of lodging for barley. J Agron Crop Sci 192:151–158

Blackburn P, Petty JA (1988) An assessment of the static and dynamic factors involved in windthrow. Forestry 61:29–43

Carter PR, Hudelson KD (1988) Influence of simulated wind lodging on corn growth and grain yield. J Prod Agric 1: 295–299

Coutts MP (1983) Root architecture and tree stability. Plant Soil 71:171–188

Crook MJ, Ennos AR (1993) The mechanics of root lodging in winter wheat, *Triticum aestivum L*. J Exp Bot 44:1219–1224

Dassault Systèmes (2014) Abaqus User's Manual v6.14. Simulia, Providence

Ennos AR, Crook MJ, Grimshaw C (1993) The anchorage mechanics of maize, *Zea mays*. J Exp Bot 44:147–153

Finnigan JJ (2000) Turbulence in plant canopies. Annu Rev Fluid Mech 32:519–571

Flesch TK, Grant RH (1991) The translation of turbulent wind energy to individual corn plant motion during senescence. Boundary Layer Meteorology 55:161–176

Goodman AM, Ennos AR (1996) A comparative study of the response of the roots and shoots of sunflower and maize to mechanical stimulation. J Exp Bot 47:1499–1507

Goodman AM, Ennos AR (1999) The effects of soil bulk density on the morphology and anchorage mechanics of the root systems of sunflower and maize. Ann Bot 83:293–302

Griffin (1998) Assessing lodging risk in winter wheat. PhD dissertation, University of Nottingham, Nottingham, UK

Horn R, Lebert M (1994) Soil compaction in crop production. In: Sloane BD, van Ouwerkerk C (eds) Soil Compaction in Crop Production. Elsevier, Amsterdam, pp 45–69

Liu S, Song F, Liu F, Zhui X, Xu H (2012) Effect of Planting Density on Root Lodging Resistance and its Relationship to Nodal Root Growth Characteristics in Maize (Zea mays L.) J Agric Sci 4:182–189

Lu SS, Willmarth WW (1974) Measurements of the structure of the Reynolds stress in a turbulent boundary layer. J Fluid Mech 670:481–511

Manzur ME, Hall AJ, Chimenti CA (2014) Root lodging tolerance in Helianthus annus (L.): associations with morphological and mechanical attributes of roots. Plant Soil 2014:71–83

Martinez-Vazquez P (2016) Crop lodging induced by wind and rain. Agric For Meteorol 228-229:265–275

Miller LA (2005) Structural dynamics and resonance in plants with nonlinear stiffness. J Theor Biol 2005:511–524

Niklas KJ (1992) Plant Biomechanics: An Engineering Approach to Plant Form and Function. U Chicago Press, Chicago

Oliver HR, Mayhead GJ (1974) Wind measurements in a pine forest during a destructive gale. Forestry 47:185–194

Pinthus MJ (1973) Lodging in wheat, barley, and oats: the phenomenon, its causes, and preventive measures. Adv Agron 25:209–263

Raupach MR, Thom AS (1981) Turbulence in and above plant canopies. Annu Rev Fluid Mech 13:97–129

Raupach MR, Finnigan JJ, Brunet Y (1996) Coherent eddies and turbulence in vegetation canopies: the mixing-layer analogy. Bound-Layer Meteorol 78:351–382

Robertson DJ, Smith SL, Gardunia BG, Cook DD (2014) An improved method for accurate phenotyping of corn stalk strength. Crop Sci 54:2038–2044

Shaw RH, Den Hartog G, King KM, Thurtell GW (1974) Measurements of mean wind flow and three-dimensional turbulence intensity within a mature corn canopy. Agric Meteorol 13:419–425

Spike BP, Tollefson JJ (1991) Yield response of corn subjected to Western Corn Root worm (Coleoptera: Chrysomelidae) infestation and lodging. J Econ Entomol 5:1585–1590

Sposaro MM, Berry PM, Sterling M, Hall AJ, Chimenti CA (2010) Modelling root and stem lodging in sunflower. Field Crop Res 119:125–134

Stamp P, Kiel C (1992) Root morphology of maize and its relationship to root lodging. J Agron Crop Sci 168:113–118

Sterling M, Baker CJ, Berry PM, Wade A (2003) An experimental investigation of the lodging of wheat. Agric For Meteorol 119:149–165

Stokes A, Atger RC, Bengough AG, Fourcaud T, Sidle RC (2009) Desirable plant root traits for protecting natural and engineered slopes against landslides. Plant Soil 324:1–30

Tritton DJ (1988) Physical fluid dynamics. Oxford University Press, Oxford

Von Forell G, Robertson D, Lee SY, Cook DD (2015) Preventing lodging in bioenergy crops: a biomechanical analysis of maize stalks suggests a new approach. J Exp Bot 66:4367–4371

Waldron LJ (1977) The shear resistance of root-permeated homogeneous and stratified soil. Soil Sci Soc Am J 41:843–849

Wilson NR, Shaw RH (1977) A higher order closure model for canopy flow. J Appl Meteorol 16:1197–1205

Wulfsohn D, Adams BA, Fredlund DG (1998) Triaxial testing of agricultural soils. Journal of Agricultural Engineering 69: 317–330